Atmos. Chem. Phys. Discuss., doi:10.5194/acp-2017-435, 2017
Manuscript under review for journal Atmos. Chem. Phys.
Discussion started: 22 May 2017


Atmospheric Chemistry and Physics
Open Access
EGU
Discussions

# Diagnosing $CH_4$ models using the equivalent length in the stratosphere

Zhiting Wang[1], Thorsten Warneke[1], Bart Dils[2], Justus Notholt[1], Marielle Saunois[3]

(1) Institute of Environmental Physics, University of Bremen, Germany
(2) Belgian Institute for Space Aeronomy, BIRA-IASB, Brussels, Belgium
(3) Laboratoire des Sciences du Climat et de l'Environnement, LSCE-IPSL (CEA-CNRS-UVSQ), Université Paris-Saclay, 91 191 Gif Sur Yvette, France

## Abstract

The equivalent length, a measure for mixing strength in the atmosphere, in meridional direction in the current application, is used here to investigate the causes of the atmospheric chemistry model (TM3, TM5-4DVAR and LMDz-PYVAR) biases in the stratosphere. Compared to measurements, we find that the modeled surf zone (a strongly stirred region caused by planetary wave breaking in mid-latitude stratosphere in the winter hemisphere), especially in the southern hemisphere, is not strong enough. We assume that this is due to an underestimation of the planetary wave breaking magnitude in the models. Consequently, the region with meridional uniform stratospheric $CH_4$ concentrations has smaller latitudinal coverages in the models than the measurements, especially in the southern hemisphere between June and September. During the southern winter, a region with both vertically and horizontally well mixed $CH_4$ concentrations occur between 450 and 850 K (~18 and 30 km) in surf zone latitudes. Such a region is absent in the models, and underestimations of $CH_4$ concentrations within it are visible in comparisons with measured $CH_4$ profiles. The modeled polar vortex breaks too fast and during the vortex period $CH_4$ concentration differences across its barrier are underestimated compared to the measurements.

## 1. Introduction

Methane ($CH_4$) is emitted at the surface and transported into the stratosphere in the tropics. In the stratosphere $CH_4$ is distributed by the residual circulation and mixing processes induced by wave breaking events, e.g. planetary wave breaking (McIntyre and Palmer, 1983). Chemical oxidation destructs $CH_4$ mostly in the upper stratosphere and results in a strong decline of $CH_4$ concentrations with altitudes above the tropopause. One common deficiency of the CTMs, using an Eulerian transport algorithm, as currently applied in the inverse modeling, is smoothing $CH_4$ gradients across transport barriers, such as the subtropical barrier (Trepte and Hitchman, 1992; Chen et al., 1994a; Neu et al., 2003) and the polar barrier (Chen et al., 1994b; Steinhorst et al., 2005) in the stratosphere, and the tropopause itself as a barrier for the stratosphere-troposphere exchange. Using a Langrangian transport scheme, the CTMs give much better performances in representing large $CH_4$ gradients across these transport barriers in the stratosphere (Stenke et al., 2009; Hoppe et al., 2014).

Inverse modeling technique is widely used to infer $CH_4$ emissions from measured concentrations. The most frequently used measurements include $CH_4$ mixing ratios at the surface, and the total columns from satellite-based sensors (e.g., SCHIAMACHY and GOSAT). Compared to in-situ surface measurements, satellite-based instruments provide valuable information for $CH_4$ sources due to their wider spatial coverage. This larger coverage is particularly important for tropical regions where in situ measurements are not possible or sparse, such as in South America (Pison et al., 2013). However, inaccuracies in the models prevent correct extraction of the information contained within the measurements. For example inverted surface emissions change when applying different physical parameterization or different vertical resolutions (Locatelli et al., 2015). Also, model errors in the stratosphere could be aliased into inverted emissions when assimilating total column measurements. An alternative approach to avoid the CTMs deficiencies in the stratosphere is using satellites measurements that have small or no sensitivities to the stratosphere. For examples, Payne et al. (2009) describes a method that extracts the troposphere representative $CH_4$ concentrations with peak sensitivities around 500 hPa from the Tropospheric Emission Spectrometer measurements (TES). Crevoisier et al. (2013) retrieves a mid-to-upper tropospheric $CH_4$ concentration from the Infrared Atmospheric Sounding Interferometer (IASI) with atmospheric temperature constrained by the Advanced Microwave Sounding Unit (AMSU). The precision is estimated to be ~0.9%. Xiong et al. (2013) retrieves mid-upper tropospheric $CH_4$ from IASI (its most sensitive layer is between 100-600 hPa in the tropics and 200-750 hPa in the extratropics). Worden et al. (2015) also presents lower tropospheric $CH_4$ retrieved through combination usage of TES and GOSAT sensors, which is estimated to have an accuracy of 10~30 ppb for a monthly average.

One of the processes that determine stratospheric tracer transports and distributions is the mixing associated with filament structures induced by wave breaking. For example, isentropic mixing processes contribute to (1) horizontally uniform tracer distributions in the surf zone, which is a region strongly stirred by planetary wave breaking in the winter stratosphere as defined by McIntyre and Palmer (1983), and (2) strong gradients of tracer concentrations at ends of the surf zone. The filament structure is one of the processes that induce exchange between air of the tropics, mid-latitudes and the polar vortex (Randel et al., 1993; Chen et al., 1994b, 1994c; Kalicinsky et al., 2013) because it increases interfaces

Atmos. Chem. Phys. Discuss., doi:10.5194/acp-2017-435, 2017
Manuscript under review for journal Atmos. Chem. Phys.
Discussion started: 22 May 2017



between air masses with different properties. Usually Eulerian models cannot represent filament structures as well as Lagrangian models (e.g. Khosrawi et al., 2005). This means that tracer transport in an Eulerian model could be not well resolved because of the important roles played by these mixing processes, such as shown by Konopka et al. (2007) and Ploeger et al. (2013). In this study the isentropic mixing in the models are evaluated with a tool called the equivalent length ($L_e$), which is introduced by Nakamura (1996) to characterize complexity of tracer distributions. In the 2D case, the equivalent length is the length of the lines of constant tracer mixing ratios if the gradient of the mixing ratios in the direction perpendicular to the isolines of the mixing ratios does not change along the isolines. Mixing processes disturb tracer contours and increase complexity of the contours and then enlarge $L_e$. The work in this study is partly presented by Wang (2016).

## 2. Models, measurements and method

Three Eulerian models evaluated here are TM3, TM5-4DVAR and LMDz-PYVAR whose resolutions are 4°×5°×26 (latitudinal and longitudinal resolution in degree, and number of vertical levels), 6°×4°×25 and 1.875°×3.75°×39, respectively. The modeled $CH_4$ 4D fields are obtained after inversion based on in situ surface measurements. The details about the global atmospheric tracer model TM3 can be found in work of Heimann and Köerner (2003) and inversion method is described by Rödenbeck (2005). TM5-4DVAR is a four-dimensional data assimilation system for inverse modeling of atmospheric methane emissions (Meirink et al., 2008). The system is based on the TM5 atmosphere transport model (Krol et al., 2005). LMDz-PYVAR is a framework that combines the inversion system PYVAR (Chevallier et al., 2005; Pison et al., 2009) with the transport model LMDz (Hourdin et al., 2006). The version used here is presented by Locatelli et al. (2015).

The measurements of stratospheric $CH_4$ profiles are those by MIPAS (Michelson Interferometer for Passive Atmospheric Sounding) (Fischer et al., 2008). MIPAS is a Fourier transform infrared (FTIR) spectrometer aboard ENVISAT for the detection of limb emission spectra in the middle and upper atmosphere. It acquires spectra over the range 685 to 2410 cm$^{-1}$. The primary geophysical parameters of interest are vertical profiles of atmospheric pressure, temperatures, and volume mixing ratios of about 25 trace constituents. The product used here is operational V6 data processed by ESA. For comparison with the models, modeled 3D fields are extracted at each measurement record through spatial and temporal interpolations.

The definition of the equivalent length, $L_e$, is:

Atmos. Chem. Phys. Discuss., doi:10.5194/acp-2017-435, 2017
Manuscript under review for journal Atmos. Chem. Phys.
Discussion started: 22 May 2017


$$L_e^2(A,t)=(\partial q/\partial A)^{-2}\partial\langle|\nabla q|^2\rangle/\partial A ,$$

where $q$ is the tracer mixing ratio ($CH_4$ in this study), the operator $\langle\ \rangle$ denotes areal integral over the region bounded by a $q$ isoline and $A$ is the bounded area by this contour. To apply this definition on the MIPAS data, $CH_4$ mixing ratios at a constant potential temperature are binned per month due to the small sampling density and noise of the measurements. Then a $CH_4$ field with a 4°×4° resolution is constructed at this isentropic surface through fitting a surface at each grid point to the collected concentrations which locate within ±3° latitude and ±5° longitude of that point. The derived $CH_4$ concentration distributions are interpolated onto a 1°×1° resolution and $L_e$ is calculated as described by Nakamura and Ma (1997). The procedure includes building $CH_4$ mixing ratio distributions as a function of the area $A$ bounded by constant $CH_4$ mixing ratios, the function $q(A, t)$ in the equation, the calculation of horizontal gradients of $CH_4$ and the areal integral of the gradient square for each $CH_4$ mixing ratio. The $CH_4$ concentration is a function of $A$, and so is the areal integral of the gradient square. Using all these quantities the $L_e^2$ is obtained according to the aforementioned definition. The equivalent latitude $\phi_e$ is defined by $A=2\pi a^2(1-\sin\phi_e)$, where $a$ is the earth radius. The quantity used to represent mixing strength here is $\widetilde{L}_e=\ln\left(L_e^2/(2\pi a\cos\varphi_e)^2\right)$ but is still called the equivalent length $L_e$ from now on for convenience. $L_e$ is calculated on surfaces of constant potential temperature ranging from 450 to 2000 K (~18 to 49 km) for each month during the period 2009-2011 for both the models and satellite data.

## 3. Characteristics of the bias in the modeled stratospheric $CH_4$

An example of the zonal mean stratospheric $CH_4$ mixing ratios during April 2011 is shown in Fig. 1. The MIPAS measurements show an uplift region with relatively high $CH_4$ mixing ratios in the tropics (25°S~25°N) between 400 to 1100 K. This is the tropical reservoir, which has weak mixing with extratropical air (Trepte and Hitchman, 1992). In the models the high $CH_4$ mixing ratio region in the tropics, however, has a lower vertical extent and a leaking boundary compared to MIPAS. The contrast in $CH_4$ mixing ratios between interior and exterior of the reservoir depends partly on the strength of the subtropical barrier and mixing processes in the extratropics. The formation of gradients in tracer mixing ratios results from differential mixing strengths, with weak mixing in the barrier region and strong mixing in one or both sides of the barrier (Nakamura, 1996, 1997). This mechanism occurs at both the subtropical barrier and the polar barrier (a region with strong tracer gradients which separates air inside the polar vortex with that in the mid-latitudes). During the months Jun. to Nov. there is a region 600-

Atmos. Chem. Phys. Discuss., doi:10.5194/acp-2017-435, 2017
Manuscript under review for journal Atmos. Chem. Phys.
Discussion started: 22 May 2017

Atmospheric Chemistry and Physics
Discussions

1000 K (~23-34 km) over the southern mid-latitudes where $CH_4$ mixing ratio is underestimated by all the models (up to 300 ppb), Some examples are shown in Fig. S1-S3 (figures with notation Fig. S# are included in the supplementary). During Jun. to Nov. horizontal mixing is strong and the surf zone is formed there. The models underestimate gradients in $CH_4$ mixing ratio across the southern polar barrier during the polar vortex period, which is most significant for TM5-4DVAR and least for LMDz-PYVAR (see Fig. S1-S3 and Fig. 4). Such biases occur at the northern polar barrier as well (Fig. 4).

# 4. Diagnosing isentropic mixing strength

In this section the strength of isentropic mixing in the models is evaluated against MIPAS measurements. The isentropic mixing strength, quantified with $L_e$, is calculated from MIPAS measured $CH_4$ fields and from the model simulations in the stratosphere as detailed in Section 2. Over a year, the polar vortex breaks and rebuilds in both southern and northern hemispheres. We aim to assess how well the models follow these processes because stratospheric tracer distributions are largely influenced by the polar vortex and mixing processes outside of it and during its break. Large $L_e$ means "important mixing" and small $L_e$ means "weak mixing".

## 4.1. $L_e$ comparison with previous work

Figure 2 shows the distribution of stratospheric $CH_4$, $L_e$ and mean zonal wind (from reanalysis datasets ERA-interim) between October 2009 and August 2010 (every other month) for the MIPAS measurements and TM5-4DVAR model (as an example, see results for all the models in Fig. S4).

From the MIPAS measurements, the largest $L_e$ is found in the extratropics but important $L_e$ values are observed in the latitudes 30°S-30°N as well, which is inconsistent with the results shown by Haynes and Shuckburgh (2000). In their modelled tracer fields, the tropics are usually a calm region. However large $L_e$ does not always mean strong isentropic mixing, and can be produced from diabatic movements as well. Motions crossing isentropic surfaces produce anomalies on $CH_4$ contours on an isentropic surface due to decreasing $CH_4$ mixing ratios with altitudes. In the upper stratosphere there are diabatically vertical motions associated with the semiannual oscillation (SAO) (Kennaugh et al., 1997). Indeed, there are some correlations between the large $L_e$ and the double peak structure in zonal mean contours of $CH_4$ mixing ratios in the tropical stratosphere according to the three years results (see the $CH_4$ mixing ratio distribution in Fig. 1 and $L_e$ in Fig. 2 for April 2010). In April/May of the three years there is large $L_e$ almost symmetrically distributed in the two hemispheres in the tropics above 850 K (e.g., the April 2010 in Fig. 2). According to previous study (Randel et al., 1998) the double peak structure in $CH_4$ mixing ratio distributions is the most significant during these months and occurred at altitudes above 10

Atmos. Chem. Phys. Discuss., doi:10.5194/acp-2017-435, 2017
Manuscript under review for journal Atmos. Chem. Phys.
Discussion started: 22 May 2017



hpa (~30 km and 850 K). Except for the diabatic motions, isentropic mixing is possible in the tropical stratosphere. The vertical motions in SAO result from zonal forces due to wave breaking events. Another example is the 2-day wave (Rojas and Norton, 2007), which peaks in the mesosphere and can propagate downward to 40 km (~1350 K) and has the maximum meridional perturbation at the equator. Another difference with the results of Haynes and Shuckburgh (2000) is the high $L_e$ poleward of 70°S/N. In their simulation, mixing in both regions is really weak. According to Chen et al. (1994b) strong stirring could exist inside the polar vortex but the strongest stirring locates in the surf zone.

### 4.2. Annual cycle in $L_e$ between Oct. 2009 and Aug. 2010

As revealed by MIPAS data in Fig. 2, in Oct. 2009 the southern polar vortex is strong and large meridional $CH_4$ gradients occur around 60°S, but starts to break at levels around 1250 K (~38 km) since isolines of $CH_4$ mixing ratios bend toward the pole there. The surf zone, which is formed by wave breaking of planetary waves propagating upward from the troposphere, is found approximately in latitudes 60°S-30°S. The planetary wave breaking results into isentropic mixing of tracers, and then a meridional uniform distribution of the tracers. The measured large $L_e$ and uniform $CH_4$ mixing ratios with respect to latitudes in the surf zone is consistent with our knowledge. However, between 450-850 K (about 18-30 km) the $CH_4$ mixing ratio in the surf zone is also almost uniform in the vertical direction. Actually this uniform region occurs earlier than Oct. (in August) and lasts until spring 2010 as shown in Fig. 3. There should be vertical mixing in that region since $CH_4$ mixing ratios generally decrease with altitudes in the stratosphere. Some gravity-type waves could be the source of the vertical disturbances instead of planetary waves. In Oct. 2009, the polar barrier appears in the southern hemisphere with small $L_e$ between the polar vortex and the surf zone. At about 45°N the northern surf zone starts to develop in this month as indicated by a horizontally narrow and vertically long zone, with slightly larger $L_e$ than its surroundings, mostly visible in levels 650-1850K.

Considering model performances, the polar vortex and surf zone are more or less represented in the southern hemisphere. The models give a weaker than measured mixing in the surf zone and $CH_4$ mixing ratios decrease across the polar barrier is better represented by LMDz-PYVAR (Fig. S4) compared to the other two models. The region with both horizontally and vertically well-mixed $CH_4$ (within 450-850 K and 60°S-30°S) is completely absent in the models (Fig. 2, 3 and S4) during the surf zone period. The larger vertical gradients in $CH_4$ mixing ratios in the models compared to the observation are more clearly shown in Fig. 3 (representing the southern mid latitudes). This absence of the vertically uniform region is visible as a negative region of the model to the measurements differences during the JJA and SON period (see Fig. S1-S3). The tropical region with large $L_e$ is the best represented by TM5-4DVAR

Atmos. Chem. Phys. Discuss., doi:10.5194/acp-2017-435, 2017
Manuscript under review for journal Atmos. Chem. Phys.
Discussion started: 22 May 2017


and LMDz-PYVAR, which capture the double peak structure of $CH_4$ mixing ratio distributions to the largest extent (not shown).

In December 2009 the southern polar vortex is already broken, and the zonal wind changes to easterlies (Fig. 2). Strong mixing occurs in the whole extratropics, and the polar barrier with small $L_e$ disappears. This is consistent with the strengthening of planetary wave breaking during polar vortex breaking because of the development of weak zonal winds (Holton, 2004, p. 424-429). However, southern $CH_4$ is still not well mixed horizontally at this time below 900 K (~31 km). In the northern hemisphere the polar vortex, polar barrier and surf zone are well defined in December. The surf zone seems to split into two regions above 850 K (~30 km) with smaller $L_e$ in the region between them, or is extending toward the tropics. Similar but less significant compared to the southern hemisphere, a region (about 20°N-60°N and 450-850 K) with small gradients in both vertical and horizontal directions occurs. In the models southern $CH_4$ is unrealistically uniform in the horizontal direction southward of 30°S, but the northern surf zone is represented well. Again TM3 and LMDz-PYVAR better capture the $CH_4$ concentration decrease across the northern polar barrier compared to TM5-4DVAR (see Fig. S4 and Fig. 4).

The northern polar vortex breaks above 1050 K (~35 km) in Feb. 2010 and strong stirring occurs as in the southern hemisphere in December 2009 (Fig. 2). However, the northern polar vortex is reestablished in April but now less potent (the polar barrier is now located northward of 75°N) and without the polar westerly jet. During this period only weak easterlies (with a maximum of 10 m/s in February and below in April) occur northward of 60°N. The surf zone become wider (30°N~70°N) and shows stronger isentropic mixing in April than in February (about 35°N~45°N). The stronger mixing is consistent with weakened westerlies that are suitable for quasi-stationary planetary wave propagation and breaking. In the southern hemisphere the situation in February is similar to that in December. But the large $L_e$ could result from remnants from the southern polar vortex breaking (Hess, 1991) instead of strong stirring since stationary planetary wave can not propagate in easterlies.

The model simulations show $CH_4$ and $L_e$ patterns similar to measurements in February and April of 2010. The $L_e$ southward of 60°S is underestimated in the models in February. That could reflect a too fast dissipation of polar vortex remnants. The reappearance of the northern polar vortex in April 2010 is represented by TM3 and LMDz-PYVAR but the contrast in simulated $CH_4$ concentration between outside and inside is too weak. A narrow and weak mixing region in the two models replaces the wide and strong stirring surf zone. TM5-4DVAR modelled $CH_4$ is completely uniform in the horizontal direction northward of ~60°N.

Atmos. Chem. Phys. Discuss., doi:10.5194/acp-2017-435, 2017
Manuscript under review for journal Atmos. Chem. Phys.
Discussion started: 22 May 2017

Atmospheric Chemistry and Physics Discussions

In June 2010 the polar vortex has disappeared in the northern hemisphere with a strongly stirred region northward of 50°N and easterlies established. In the southern hemisphere the polar vortex and surf zone start to build. The developing isentropic stirring in the mid-latitudes mixed with the deceasing tropical large $L_e$ region at that time. The more complete developing process of the surf zone can be seen from Fig. 3. Propagation of the planetary waves starts around 40°S at 450 K level and tilts along isolines of zonal wind, consistent with the theory that the quasi-stationary planetary wave propagates in westerlies is no stronger than a threshold (Holton, 2004, p. 424). That is reflected in the LMDz-PYVAR well, but with significant underestimated amplitudes in the other two models.

In August 2010 the polar vortex and surf zone are matured in the southern hemisphere. The models roughly capture the meridional distribution of southern $CH_4$. The deficiencies of the models are too weak isentropic mixing in the surf zone. Large departures in $L_e$ occur at the level around 1050 K and below 700 K (~26 km) in the mid-latitudes.

### 4.3. Evolution of $CH_4$ concentration and $L_e$ on isentropic surfaces in the southern mid-latitudes

Figure 3 gives the evolution of $L_e$ and $CH_4$ mixing ratios in the southern mid-latitudes (35°S-55°S) from the MIPAS measurements and the three models. As said before, the models underestimate mixing strength in the surf zone. But this underestimation differs from year to year, e.g. the models perform better in 2009 and 2011 than 2010. In the measurement, the surf zone starts in May at 450 K level and hereafter extends upward into the mid- and upper- stratosphere. In the models, the surf zone occurs later compared to the measurement. The large $L_e$ regions (about 450-850 K initially and the vertical extent decreases with time) extend into next spring in the measurement in contrast to a sudden disappearance in the models after the end of each year. As explained in Sect. 4.2, the large $L_e$ could come from remnants of strong disturbances during polar vortex breaking since easterlies of zonal wind have established in that time. There is a strong mixing region moving downward from the upper stratosphere and finally mixing into the developing surf zone, which is shown in the measurement only. That could be associated with the SAO mentioned in Sect. 4.2.

The distribution of $CH_4$ concentrations and the meridional gradients, and $L_e$ at 600 K (~24 km) as a function of latitudes in the period 2009-2011 is given in Fig. 4 to further reveal the model deficiencies in representing the surf zone development and the polar vortex breaking. The surf zone (the mid-latitudes beside the band with strong meridional gradients of $CH_4$ concentrations) mixing is weaker in all the models compared to the observation. In 2010 and 2011, the biases in the modeled mixing strength in the surf zone are more important than during 2009 in latitudes between about 30°-60°, when polar vortexes are well defined in $CH_4$ distributions. Consequently, the region with small meridional gradients (<5 ppb/degree) in $CH_4$ mixing ratios has smaller latitudinal and temporal coverage in 2010 and 2011. The polar barrier (band with large meridional gradients in $CH_4$ concentrations around 60°) is stronger in the measurements compared to the models, particularly for TM5-4DVAR. Although low $CH_4$ concentrations in the polar vortex result from sink down motion, the tight boundary could have an attribution to mixing processes both inside and outside of the polar vortex. The stronger the mixing at both sides of a transport barrier is, the tighter the barrier appears in a tracer distribution. The role of mixing in the barrier formation can be seen in the subtropical barrier (the ~30° latitudes with local maximum meridional gradients in $CH_4$ mixing ratios), which is meridionally narrower in the measurements than in the models. The mixing inside the southern polar vortex has similar/larger strength in the models but covers a smaller latitudinal range as compared to the observation. Strong meridional shear of zonal wind could be a source of the disturbances inside the polar vortex. It is not clear whether other sources contribute as well.

## 5. Discussions and conclusions

The region with both vertical and meridional uniform $CH_4$ distributions in southern mid-latitudes is located just above the subtropical jet at the tropopause. The jet exit region is recognized as a favored location for large-amplitude, subsynoptic gravity waves (Plougonven and Zhang, 2013). Such a jet system occurs in the northern hemisphere in winter as well, but there is no, or insignificant, region with uniform $CH_4$ mixing ratios above the jet. The main sources of gravity waves include orography, convection, and jet/front system. The strength of these sources is larger or the same in the northern hemisphere compared to the southern hemisphere. It is not clear what factors contribute to the difference in $CH_4$ distributions above the winter jet between the two hemispheres. The horizontal scales of the gravity waves typically range from 10 to 1000 km. The horizontal resolutions of 2°-6° of the models, which represent waves with wavelength longer than ~600 km only, is not fine enough to resolve gravity waves completely.

Isentropic mixing in the surf zone is too weak in the models compared to the observation. Reasons could be an underestimation of the planetary wave strength or deficiencies in describing the dissipation processes of the wave. In the southern hemisphere convection is an important source for the planetary wave, but orography plays a role in the northern hemisphere as well. Filament structures occur in breaking processes of planetary waves, the smaller $L_e$ in the models than in the observations indicate the fine-scale structure is smeared out partly. The ability of models to preserve fine-scale structure depends on both the resolution and transport scheme. For example the finite-volume scheme (Van Leer, 1977) as applied in LMDz is originally designed for resolving sharp gradients and discontinuities and is expected to describe the filament structures better than the slope scheme (Russel and Lerner, 1981) used in TM3. Sensitivity tests, such as changing horizontal resolutions, using different advection algorithms and convection parameterization schemes could be helpful to clarify the dominant factor leading to model biases in the surf zone.

The polar barrier is not as tight in the models as in the observation. That could be due to the inability of the models to simulate mixing processes both inside and outside of the polar vortex. The contrasts in $CH_4$ mixing ratios inside and outside of the polar vortex are better preserved by LMDz-PYVAR. The reason could be that LMDz uses a sharp-gradient-preserved transport scheme and a finer resolution. The looser barrier could be a reason for faster dissipation of the polar vortex in the model. The polar vortex is frequently forced away from the pole and sometimes to lower latitudes during the dissipation period. Unrecognized remains of the polar vortex in the model could cause problems when assimilating total column measurements.

## Code availability

The model outputs of TM3, TM5-4DVAR and LMDz-PYVAR are provided by other institutes. The corresponding PIs (see Data availability section) should be contacted for the availability of the model codes.

## Data availability

The model outputs are from Marille Saunois (Laboratoire des Sciences du Climat et de l'Environnement, France) for LMDz-PYVAR, Ute Karstens (the Max Plank Institute for Biogeochemistry, Jena, Germany) for TM3, and Peter Bergamaschi (European Commission Joint Research Centre) for TM5-4DVAR. One should contact these authors directly considering the availability the model output. The MIPAS data is operational V6 data processed by ESA, which is publicly available.

## Acknowledgements

We thank Ute Karstens at the Max Plank Institute for Biogeochemistry, Jena, Germany for providing TM3 model data and Peter Bergamaschi at European Commission Joint Research Centre for providing TM5-4DVAR data.

Atmos. Chem. Phys. Discuss., doi:10.5194/acp-2017-435, 2017
Manuscript under review for journal Atmos. Chem. Phys.
Discussion started: 22 May 2017


## References

Bernath, P. F., McElroy, C. T., Abrams, M. C., et al.: Atmospheric Chemistry Experiment (ACE): Mission overview, Geophys. Res. Lett., 32, L15S01, 2005.

Chen, P., Holton, J. R., O'neill, A. and Swinbank, R.: Isentropic Mass Exchange between the Tropics and Extratropics in the Stratosphere, J. Atmos. Sci., 51(20), 3006–3018, 1994a.

Chen, P., Holton, J. R., O'neill, A. and Swinbank, R.: Quasi-horizontal transport and mixing in the Antarctic stratosphere, J. Geophys. Res., 99(D8), 16851, doi:10.1029/94jd00784, 1994b.

Chen, P.: The permeability of the Antarctic vortex edge, J. Geophys. Res., 99(D10), 20563, doi:10.1029/94jd01754, 1994c.

Crevoisier, C., Nobileau, D., Armante, R., Crépeau, L., Machida, T., Sawa, Y., Matsueda, H., Schuck, T., Thonat, T., Pernin, J., Scott, N. A., and Chédin, A.: The 2007–2011 evolution of tropical methane in the mid-troposphere as seen from space by MetOp-A/IASI, Atmos. Chem. Phys., 13, 4279-4289, doi:10.5194/acp-13-4279-2013, 2013.

Chevallier, F., Fisher, P., Serrar, S., Bousquet, P., Breon, F.-M., Chedin, A., and Ciais, P.: Inferring $CO_2$ sources and sinks from satellite observations: Method and application to TOVS data, J. Geophys. Res., 110, D24309, doi:10.1029/2005JD, 2005.

Fischer, H., Birk, M., Blom, C., Carli, B., Carlotti, M., von Clarmann, T., Delbouille, L., Dudhia, A., Ehhalt, D., Endemann, M., Flaud, J. M., Gessner, R., Kleinert, A., Koopman, R., Langen, J., López-Puertas, M., Mosner, P., Nett, H., Oelhaf, H., Perron, G., Remedios, J., Ridolfi, M., Stiller, G., and Zander, R.: MIPAS: an instrument for atmospheric and climate research, Atmos. Chem. Phys., 8, 2151-2188, doi:10.5194/acp-8-2151-2008, 2008.

Hoppe, C. M., Hoffmann, L., Konopka, P., Grooß, J.-U., Ploeger, F., Günther, G., Jöckel, P. and Müller, R.: The implementation of the CLaMS Lagrangian transport core into the chemistry climate model EMAC 2.40.1: application on age of air and transport of long-lived trace species, Geosci. Model Dev., 7(6), 2639–2651, doi:10.5194/gmd-7-2639-2014, 2014.

Heimann, M., and S. Körner, The Global Atmospheric Tracer Model TM3: Model description and users manual release 3.8a, Tech. Rep. 5, Max Planck Inst. for Biogeochem., Jena, Germany, 2003.

Hourdin, F., Musat, I., Bony, S., Braconnot, P., Codron, F., Dufresne, J. L., Fairhead, L., Filiberti, M. A., Friedlingstein, P., Grandpeix, J. Y., Krinner, G., Li, Z. X., and Lott, F.: The LMDz4 general circulation model: climate performance and sensitivity to parametrized physics with emphasis on tropical convection, Climate Dynamics, 27, 787-813, 2006.

Haynes, P. and Shuckburgh, E.: Effective diffusivity as a diagnostic of atmospheric transport: 1. Stratosphere, J. Geophys. Res., 105(D18), 22777–22794, doi:10.1029/2000jd900093, 2000.

Hess, P. G.: Mixing Processes Following the Final Stratospheric Warming, J. Atmos. Sci., 48(14), 1625–1641, 1991.

Holton, J. R.: An Introduction to Dynamic Meteorology, fourth edition, International Geophysics Series, Elsevier Academic Press, 88, 2004.

Kalicinsky, C., Grooß, J.-U., Günther, G., Ungermann, J., Blank, J., Höfer, S., Hoffmann, L., Knieling, P., Olschewski, F., Spang, R., Stroh, F., and Riese, M.: Observations of filamentary structures near the vortex edge in the Arctic winter lower stratosphere, Atmos. Chem. Phys., 13, 10859-10871, doi:10.5194/acp-13-10859-2013, 2013.

Khosrawi, F., Grooß, J.-U., Müller, R., Konopka, P., Kouker, W., Ruhnke, R., Reddmann, T. and Riese, M.: Intercomparison between Lagrangian and Eulerian simulations of the development of mid-latitude streamers as observed by CRISTA, Atmos. Chem. Phys., 5(1), 85–95, doi:10.5194/acp-5-85-2005, 2005.

Konopka, P., Günther, G., Müller, R., dos Santos, F. H. S., Schiller, C., Ravegnani, F., Ulanovsky, A., Schlager, H., Volk, C. M., Viciani, S., Pan, L. L., McKenna, D.-S., and Riese, M.: Contribution of mixing to upward transport across the tropical tropopause layer (TTL), Atmos. Chem. Phys., 7, 3285-3308, doi:10.5194/acp-7-3285-2007, 2007.

Krol, M., Houweling, S., Bregman, B., van den Broek, M., Segers, A., van Velthoven, P., Peters, W., Dentener, F., and Bergamaschi, P.: The two-way nested global chemistry-transport zoom model TM5: algorithm and applications, Atmos. Chem. Phys., 5, 417-432, doi:10.5194/acp-5-417-2005, 2005.

Kennaugh, R., Ruth, S. and Gray, L. J.: Modeling quasi-biennial variability in the semiannual double peak, J. Geophys. Res., 102(D13), 16169–16187, doi:10.1029/97jd00867, 1997.

Mcintyre, M. E. and Palmer, T. N.: Breaking planetary waves in the stratosphere, Nature, 305(5935), 593–600, doi:10.1038/305593a0, 1983.

Meirink, J. F., Bergamaschi, P., and Krol, M. C.: Four-dimensional variational data assimilation for inverse modelling of atmospheric methane emissions: method and comparison with synthesis inversion, Atmos. Chem. Phys., 8, 6341-6353, doi:10.5194/acp-8-6341-2008, 2008.

Neu, J. L.: Variability of the subtropical "edges" in the stratosphere, J. Geophys. Res., 108(D15), doi:10.1029/2002jd002706, 2003.

Nakamura, N.: Two-Dimensional Mixing, Edge Formation, and Permeability Diagnosed in an Area Coordinate, J. Atmos. Sci., 53(11), 1524–1537, 1996.

Nakamura, N. and Ma, J.: Modified Lagrangian-mean diagnostics of the stratospheric polar vortices: 2. Nitrous oxide and seasonal barrier migration in the cryogenic limb array etalon spectrometer and SKYHI general circulation model, Journal of Geophysical Research: Atmospheres J. Geophys. Res., 102(D22), 25721–25735, 1997.

Pison, I., Bousquet, P., Chevallier, F., Szopa, S., and Hauglustaine, D.: Multi-species inversion of $CH_4$, CO and $H_2$ emissions from surface measurements, Atmos. Chem. Phys., 9, 5281-5297, doi:10.5194/acp-9-5281-2009, 2009.

Pison, I., Ringeval, B., Bousquet, P., Prigent, C. and Papa, F.: Stable atmospheric methane in the 2000s: key-role of emissions from natural wetlands, Atmos. Chem. Phys., 13(23), 11609–11623, doi:10.5194/acp-13-11609-2013, 2013.

Payne, V. H., Clough, S. A., Shephard, M. W., Nassar, R., and Logan, J. A.: Information-centered representation of retrievals with limited degrees of freedom for signal: Application to methane from the Tropospheric Emission Spectrometer, J. Geophys. Res., 114, D10307, doi:10.1029/2008JD010155, 2009.

Ploeger, F., Günther, G., Konopka, P., Fueglistaler, S., Müller, R., Hoppe, C., Kunz, A., Spang, R., Grooß, J.-U. and Riese, M.: Horizontal water vapor transport in the lower stratosphere from subtropics to high latitudes during boreal summer, J. Geophys. Res., 118(14), 8111–8127, doi:10.1002/jgrd.50636, 2013.

Plougonven, R. and Zhang, F.: Internal gravity waves from atmospheric jets and fronts, Rev. Geophys., 52(1), 33–76, doi:10.1002/2012rg000419, 2014.

Randel, W. J., Gille, J. C., Roche, A. E., Kumer, J. B., Mergenthaler, J. L., Waters, J. W., Fishbein, E. F. and Lahoz, W. A.: Stratospheric transport from the tropics to middle latitudes by planetary-wave mixing, Nature, 365(6446), 533–535, doi:10.1038/365533a0, 1993.

Rödenbeck, C., Estimating $CO_2$ sources and sinks from atmospheric mixing ratio measurements using a

Atmos. Chem. Phys. Discuss., doi:10.5194/acp-2017-435, 2017
Manuscript under review for journal Atmos. Chem. Phys.
Discussion started: 22 May 2017


Atmospheric Chemistry and Physics
Discussions
Open Access
EGU

global inversion of atmospheric transport, Technical Report 6, Max Planck Institute for Biogeochemistry, Jena, Germany, 2005.

Rojas, M. and Norton, W.: Amplification of the 2-day wave from mutual interaction of global Rossby-gravity and local modes in the summer mesosphere, J. Geophys. Res., 112(D12), doi:10.1029/2006jd008084, 2007.

Randel, W. J., Wu, F., Russell, J. M., Roche, A. and Waters, J. W.: Seasonal Cycles and QBO Variations in Stratospheric $CH_4$ and $H_2O$ Observed in UARS HALOE Data, J. Atmos. Sci., 55(2), 163–185, 1998.

Russell, G. L. and Lerner, J. A.: A New Finite-Differencing Scheme for the Tracer Transport Equation, J. Appl. Meteor., 20(12), 1483–1498, 1981.

Steinhorst, H.-M., Konopka, P., Günther, G. and Müller, R.: How permeable is the edge of the Arctic vortex: Model studies of winter 1999-2000, J. Geophys. Res., 110(D6), doi:10.1029/2004jd005268, 2005.

Stenke, A., Dameris, M., Grewe, V. and Garny, H.: Implications of Lagrangian transport for simulations with a coupled chemistry-climate model, Atmos. Chem. Phys., 9(15), 5489–5504, doi:10.5194/acp-9-5489-2009, 2009.

Trepte, C. R. and Hitchman, M. H.: Tropical stratospheric circulation deduced from satellite aerosol data, Nature, 355(6361), 626–628, 1992.

Leer, B. V.: Towards the ultimate conservative difference scheme. Part IV: A new approach to numerical convection, Journal of Computational Physics, 23(3), 276–299, 1977.

Xiong, X., Barnet, C., Maddy, E. S., Gambacorta, A., King, T. S., and Wofsy, S. C.: Mid-upper tropospheric methane retrieval from IASI and its validation, Atmos. Meas. Tech., 6, 2255-2265, doi:10.5194/amt-6-2255-2013, 2013.

Worden, J. R., Turner, A. J., Bloom, A., Kulawik, S. S., Liu, J., Lee, M., Weidner, R., Bowman, K., Frankenberg, C., Parker, R., and Payne, V. H.: Quantifying lower tropospheric methane concentrations using GOSAT near-IR and TES thermal IR measurements, Atmos. Meas. Tech., 8, 3433-3445, doi:10.5194/amt-8-3433-2015, 2015.

Wang, Z.: Remote sensing of tropospheric methane and isotopes of atmospheric carbon dioxide using Fourier Transform Spectrometry, http://elib.suub.uni-bremen.de/edocs/00105597-1.pdf, 2016

Atmos. Chem. Phys. Discuss., doi:10.5194/acp-2017-435, 2017
Manuscript under review for journal Atmos. Chem. Phys.
Discussion started: 22 May 2017


# Figures

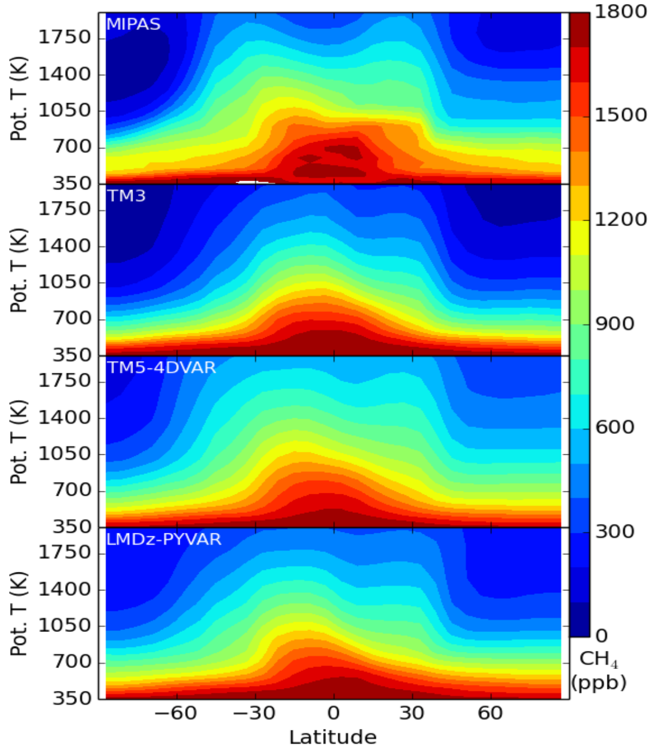


Figure 1. Zonal median $CH_4$ mixing ratios as a function of latitudes and potential temperature in April of 2010 for (from top to bottom) MIPAS, TM3, TM5-4DVAR and LMDz-PYVAR.

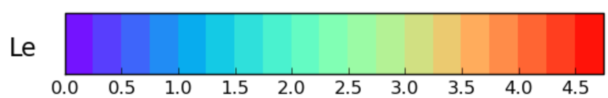

Atmos. Chem. Phys. Discuss., doi:10.5194/acp-2017-435, 2017
Manuscript under review for journal Atmos. Chem. Phys.
Discussion started: 22 May 2017


Atmospheric Chemistry and Physics
Discussions

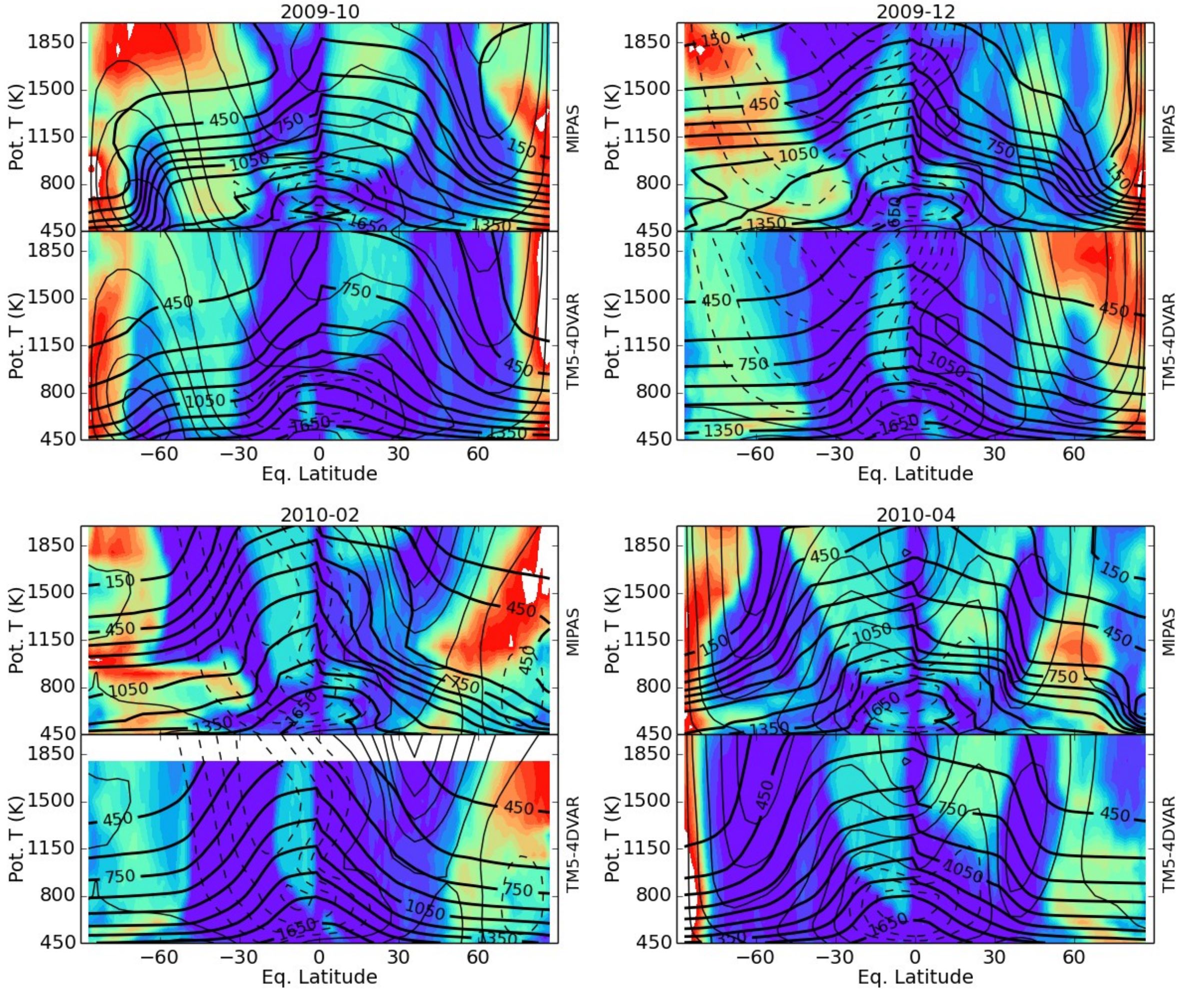

Atmos. Chem. Phys. Discuss., doi:10.5194/acp-2017-435, 2017
Manuscript under review for journal Atmos. Chem. Phys.
Discussion started: 22 May 2017



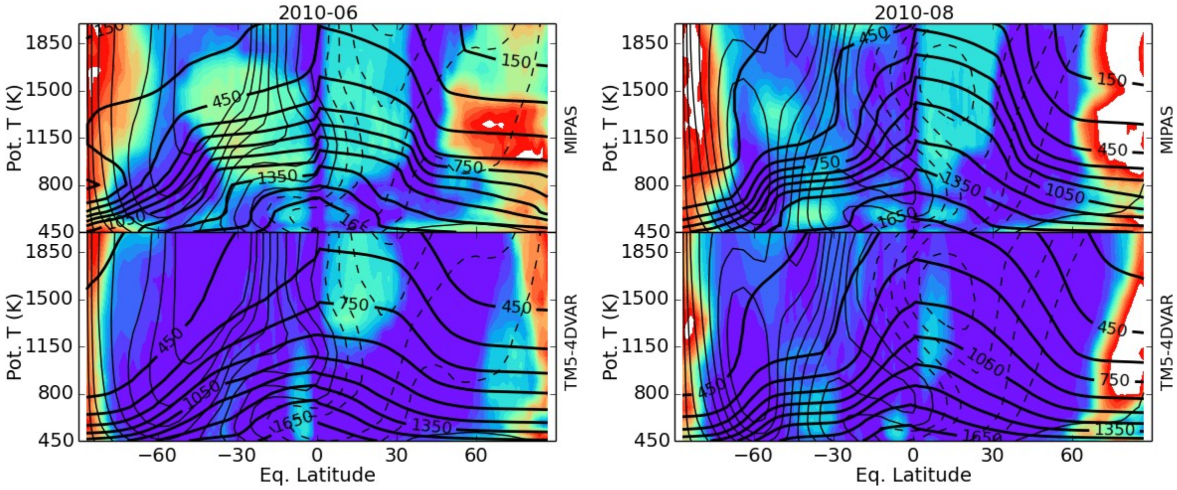


Figure 2. Distributions of $L_e$ (colors, the white means no data or larger values), $CH_4$ mixing ratios (thick black lines with increment of 100 ppb) and zonal mean zonal wind (thin black lines with solid for westerlies and zero values and dashed lines for easterlies, the increment is 10 m/s) along equivalent latitudes (but latitudes for wind) and potential temperatures. Results for MIPAS (upper panel) and TM5-4DVAR (lower panel) are shown between October 2009 and August 2010 every other month.

Atmos. Chem. Phys. Discuss., doi:10.5194/acp-2017-435, 2017
Manuscript under review for journal Atmos. Chem. Phys.
Discussion started: 22 May 2017




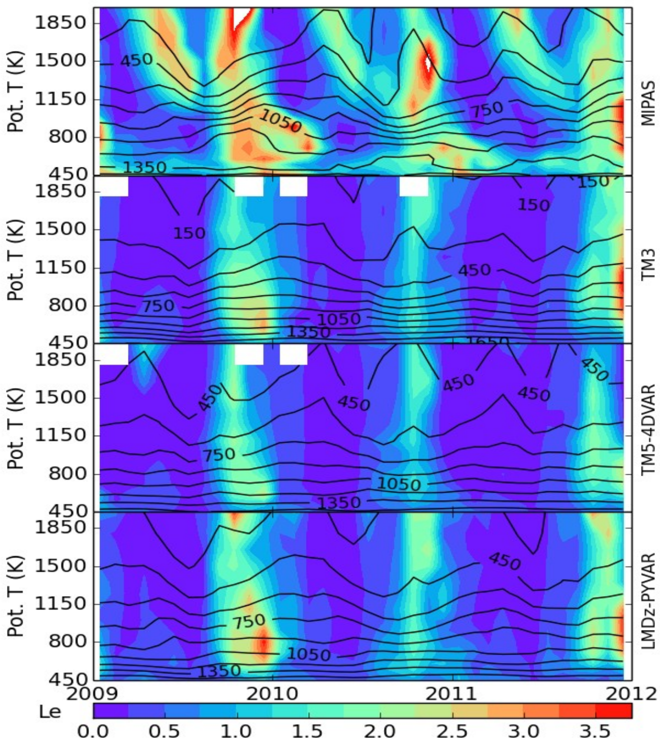


Figure 3. Evolution of the measured and modeled $L_e$ (color), and $CH_4$ mixing ratios (black lines) averaged over 35°S-55°S between January 2009 and December 2011.

Atmos. Chem. Phys. Discuss., doi:10.5194/acp-2017-435, 2017
Manuscript under review for journal Atmos. Chem. Phys.
Discussion started: 22 May 2017


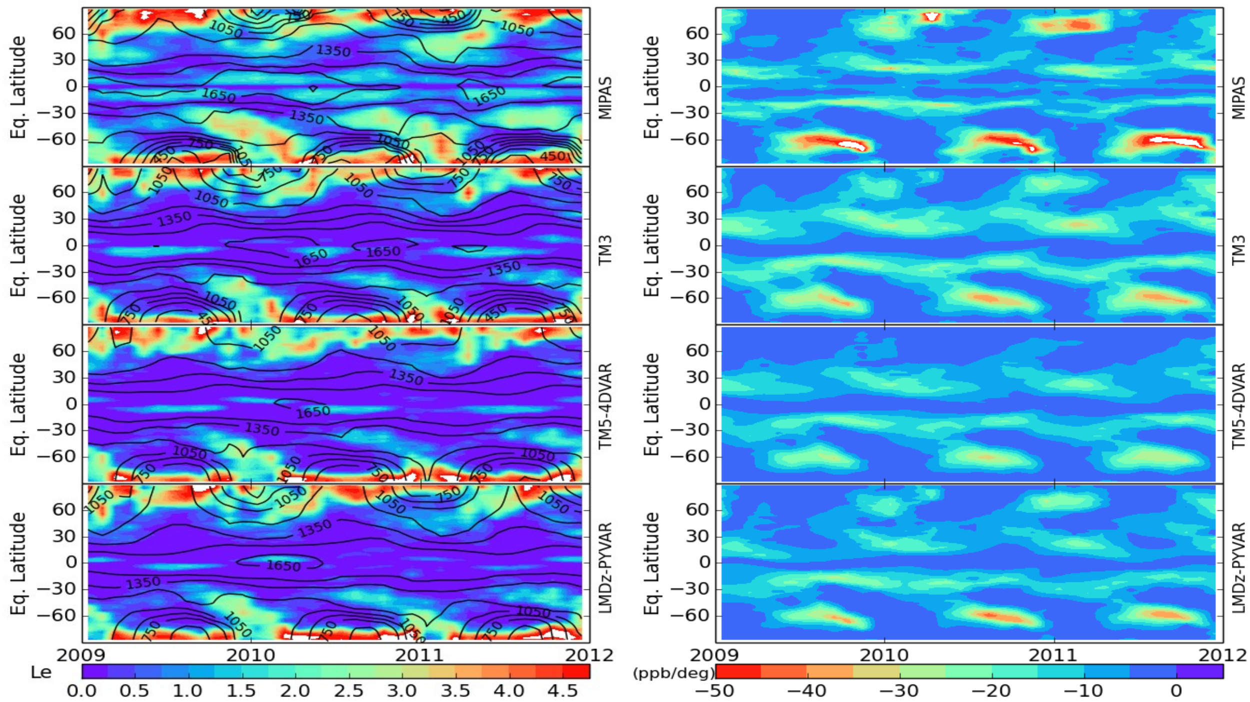


Figure 4. Right: Measured (MIPAS, uppermost panel) and modeled (TM3, TM5-4DVAR and LMDz-PYVAR) latitude-time distribution of $CH_4$ mixing ratios (black line, in ppb) and $L_e$ (color) at 600 K (~24 km). Left: meridional gradients of $CH_4$ mixing ratios (the positive means increase toward the poles) at the same potential temperature surface.